J Appl Electrochem (2014) 44:391–398
DOI 10.1007/s10800-013-0653-z

RESEARCH ARTICLE

Enhanced capacitance of a NiO electrode prepared in the magnetic field

Guo-xiang Wang · Jian Cai · Hong-feng Xu · Lu Lu · Hong Zhao

Received: 5 September 2013 / Accepted: 2 December 2013 / Published online: 18 December 2013

Abstract The enhancement of the surface alignment by magnetic field had a great theoretical and practical significance in the improvement of electrochemical capacitor. In the present study, the NiO nanowires were synthesized by liquid-phase reduction method, and the electrode was prepared within external magnetic field. The effects of magnetic field on the electrode surface and the electrochemical behavior were investigated. X-ray diffraction and scanning electron microscope studies showed that the applied magnetic field results in an orderly surface structure of the electrode, which induced an effective transfer path for the electrons and ions. Meanwhile, the orderly electrode surface improved the electrochemical capacitance, as well as decreased the internal resistance. It was found on the cyclic voltammetry and galvanostatic charge/discharge measurements that the electrode prepared with the magnetic field displays an increased capacitance (506 F g^{-1}), high power density (135.8 W kg^{-1}) and energy density (17.6 Wh kg^{-1}), and improved cycle stability compared to the electrode without magnetic field. Electrochemical impedance spectroscopy results demonstrated enhanced electrochemical properties for the addition of magnetic field.

Keywords Nickel oxide · Nanowire · Magnetic field · Supercapacitor

Foundation item: Project supported by the National Natural Science Foundation of China (Grant No. 21376034) and the National Basic Research Program of China (973 Program, Grant No. 2012CB215500).

G. Wang · H. Xu (✉) · L. Lu · H. Zhao
Liaoning Provincial Key Laboratory of New Energy Battery, Dalian Jiaotong University, Huanghe Road 794#, Dalian 116028, People's Republic of China
e-mail: hfxu@fuelcell.com.cn

G. Wang
Department of Materials and Science and Engineering, Dalian Jiaotong University, Huanghe Road 794#, Dalian 116028, People's Republic of China

J. Cai
School of Electronics and Information Engineering, Dalian Jiaotong University, Huanghe Road 794#, Dalian 116028, People's Republic of China

1 Introduction

An electrochemical supercapacitor is a new type of energy storage device between traditional capacitors and rechargeable batteries [1]. In recent years, supercapacitors have gained considerable attention in energy storage application [2–4] because of their high power density, fast charge and discharge rates, long life cycles, and cycling stability. Pseudocapacitance meets these needs in the technology platform of choice and fastly becomes the preferred power source for hybrid electric vehicles (HEVs) and plug-in hybrid vehicles [5]. The materials most commonly used as electrochemical supercapacitors are active carbons, conductive polymer, and metal oxide [6–8]. Among metal oxides, various high capacitance types of ruthenium oxides have been extensively studied for active electrode applications [9, 10].

Pseudocapacitance is an interfacial phenomenon which is closely related to the specific surface area of electroactive materials [11, 12]. Transition metal oxides are widely studied as electrochemical materials. Pseudocapacitances that employ transition metal oxides (WO_3 [13], NiO [14], MoO_3 [15], and MnO_2 [16]) to replace currently used noble metal oxides, such as RuO_2 and IrO_2, are receiving increased attention because of their superior

electrochemical behavior and low cost [17]. Nickel oxide, which is known to be friendly environment and cheap, is a promising electrode material for pseudocapacitors. The theoretical value of NiO in a potential window of 0.5 V is 2,584 F g^{-1} [18].

As important pseudocapacitors, nickel oxide nanostructured materials have a high specific surface area, which leads to the efficient paths of electrolyte ions with electroactive sites for Faradaic energy storage [19–22]. Significant efforts have been devoted to control the size and morphology of NiO to enhance capacitance. For instance, the metal oxide grain size is reduced to the nanometer scale. Mg and Si are added for NiO alloys or other heavy elements, such as W, Ta, and Co. In general, nanosized metals or alloying possess a stable crystalline structure, a large surface area-to-volume ratio, and a large electrode/electrolyte interface. However, agglomeration of particles is unavoidable, and the barrier effect of mass and electron transfers can be observed between the electrode and electrolyte.

Therefore, studies have aimed to enhance the electrochemical properties of NiO, such as 1D nanowires. Nanowires offer fluent electron transfer paths. An 1D continuous structure reduces the coverage of nanomaterials, and the fluent anisotropy network enhances mass transfer efficiently. At present, some studies use template synthesis NiO nanowires, but the route often requires removal of surfactant templating, and the template limits the length of the nanowires. In improving the length of nanowires, Shao et al. [23] found that NiO ultrafine nanowires had been produced by electrostatic spinning with polyvinyl alcohol as complexing agent and nickel acetate as precursor. Liang et al. [24] fabricated 3D nanoporous NiO films by using a two-step process through an electrochemical route. These methods improved electrochemical properties because NiO morphology was controlled, but the activity and utilization rate of the electrode material were low, and stacking and agglomeration of the electrode surface were not avoided during the preparation of the electrodes. In addition, previous findings indicated that the magnetic field affects mass transfer dynamics [25] and surface electrochemistry [26]. However, the morphology of the electrode surface controlled by the added magnetic field has not been observed. In this study, an electrode with high activity, effective specific surface area, and efficient transport paths was prepared in the magnetic field to align the magnetic particles along the magnetic induction line to prevent stacking.

This study reports the fabrication of a high-capacitance electrode by addition of magnetic field. The composition, structure, and morphology of the electrode are described. Electrochemical characterization is conducted in a three-electrode system with the use of an electrochemical workstation.

2 Experimental

2.1 Material synthesis and electrode preparation

All chemical reagents used in this experiment are of analytical grade and were received without further purification. Deionized water was used throughout the experiment. In a typical synthesis run, NiO was extracted by solvation of $NiCl_2 \cdot 6H_2O$ (0.1 g) in 38 mL ethanol mixed with 30 mL water at room temperature in an open environment. The bright solution was magnetically stirred for 3 min and heated in a water bath at 60 °C for approximately 40 min by dropping 40 mL of hydrazine hydrate ($H_2N–NH_2 \cdot H_2O$). The solid black product was harvested by centrifugation and washed with deionized water and ethanol several times before it was dried at 50 °C in an oven overnight. Subsequently, the black powder was calcined in air at 350 °C for 24 h with a temperature ramp of 1 °C per minutes.

The working electrode was prepared as follows: 80 wt% of the synthesized NiO, 15 wt% of acetylene, and 5 wt% of Nafion (total mass of 20 mg) were mixed to yield a paste. Ethanol was used as a solvent. The paste was incorporated into the nickel foam (1 × 1 cm) and dried at room temperature in a magnetic field of 0.4 T (denoted by MNiO), as shown in Fig. 1a. In the contrast experiment, the mixture was simply loaded into the nickel foam without addition of a magnetic field (denoted by NiO), as shown in Fig. 1b. Nickel foam was weighted before and after material loading to obtain the exact weight of the electroactive samples in each electrode.

2.2 Sample characterization

The crystal structures were analyzed by X-ray diffraction (XRD) equipped with a Rigaku D/max Ultima III using Cu Kα radiation (λ = 1.50405 Å). Transmission electron microscopy (TEM) images were obtained from a Philips-CM 200 at 200 kV. To investigate the morphology of the electrode surfaces, field emission scanning electron microscopy (FE-SEM) images were obtained by FE-SEM (JEOL JSM-6360FLV Microscope) at 20 kV.

Electrochemical characterization was performed by AUTOLAB (ECO CHEMIE, PGSTAT 302 N) with a standard three-electrode electrode electrochemical cell that contains a 6 M KOH aqueous solution as electrolyte at room temperature and normal pressure. The as-prepared MNiO and NiO electrodes were used as the working electrode, a platinum wire (1 mm diameter) as the counter electrode, and an Hg/Hg_2Cl_2 electrode (SCE, saturated KCl, 0.214 V vs. NHE at 25 °C) as the reference electrode. The counter and reference electrodes were purchased from INESA Instrument, Inc.

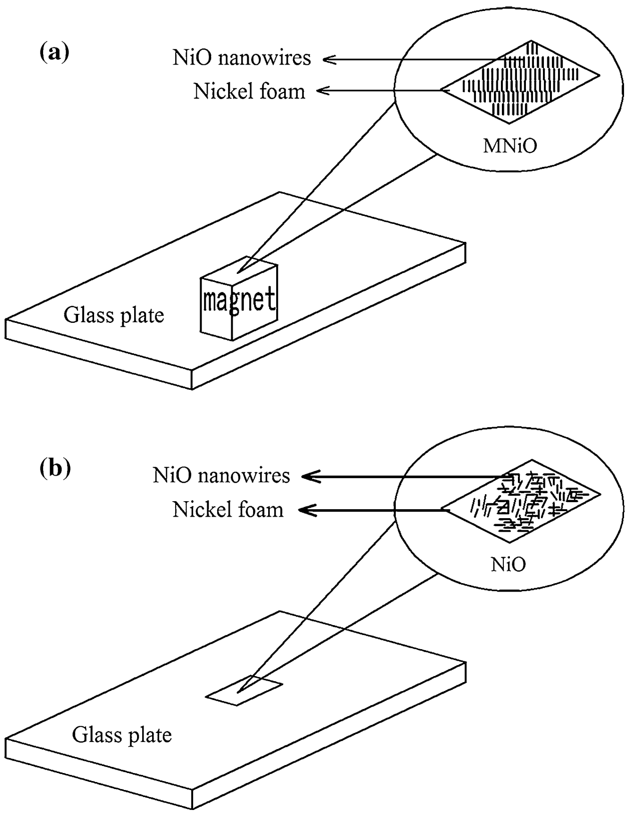

Fig. 1 Schematic diagram of electrode prepared **a** with and **b** without magnetic field

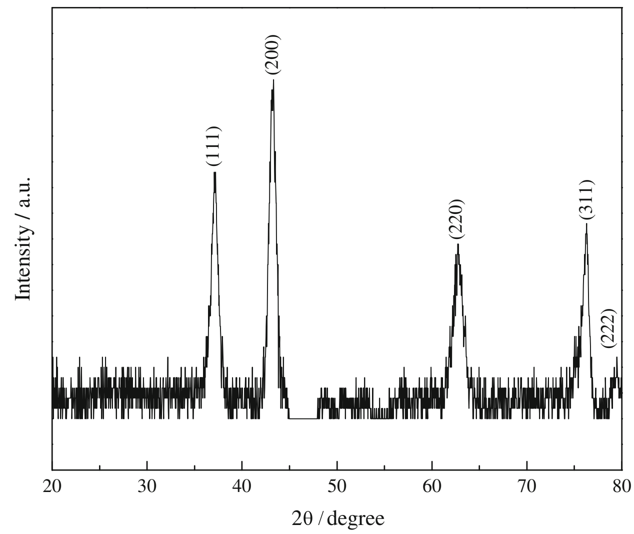

Fig. 2 XRD spectra of the NiO sample

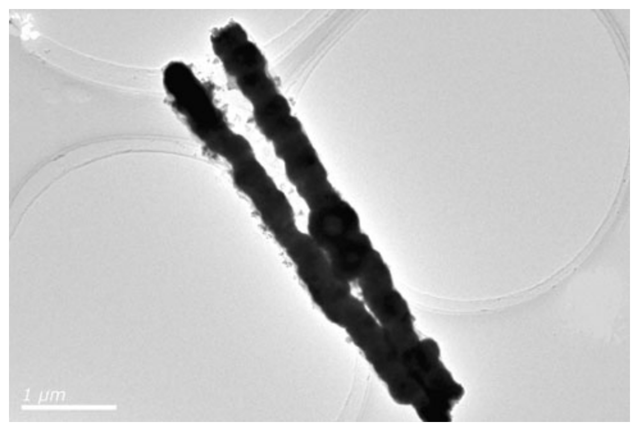

Fig. 3 HRTEM image of the NiO sample

3 Results and discussion

3.1 Structural and morphological characterizations and chemical composition of NiO and the as-prepared electrodes

The XRD pattern of the black sample obtained after calcination is shown in Fig. 2. The diffraction peaks are indexed at $2\theta = 37.2°$, 44.3°, 63.0°, 76.2°, and 79.4°, which correspond to the (110), (200), (220), (311), and (222) reflections of the NiO structures (JCPDS card No. 47-1049). So it clearly indicates that the temperature 350 °C was sufficient to convert the sample to NiO, and no peaks of impurities were observed.

To investigate the morphologies of the obtained NiO, TEM measurement was performed, and the TEM images of NiO are shown in Fig. 3. Nanowire-type structures were found in the samples. The synthesized NiO nanowires were approximately 150 nm in diameter and 4 μm in length.

To estimate the surface morphologies of the MNiO and NiO electrodes, SEM measurements were conducted, and the results are shown in Fig. 4a, b. The prepared magnetic-field-aided electrode exhibited differences. Obviously, Fig. 4 shows an orderly surface and pole structures, in which the electrode was prepared in the magnetic field. However, the surface of the electrode prepared without a magnetic field is disordered, with NiO nanowire aggregation, as shown in Fig. 4b. The effect of the magnetic field is evident in the difference between the two electrode surfaces as a result of the oriented arrangement of the magnetic NiO nanowires. These results indicate that during the production of electrodes, the addition of a magnetic field can promote directional arrangement for NiO nanowires on the electrode surface and improve the electrode specific surface area.

3.2 Electrochemical properties

Cyclic voltammetry (CV) is a method used to determine the electrochemical properties of electrodes. Figure 5a, b shows the CV curves of the electrodes at different scan rates in a 6 M KOH aqueous solution. The scan rates were 1, 5, 10, 25,

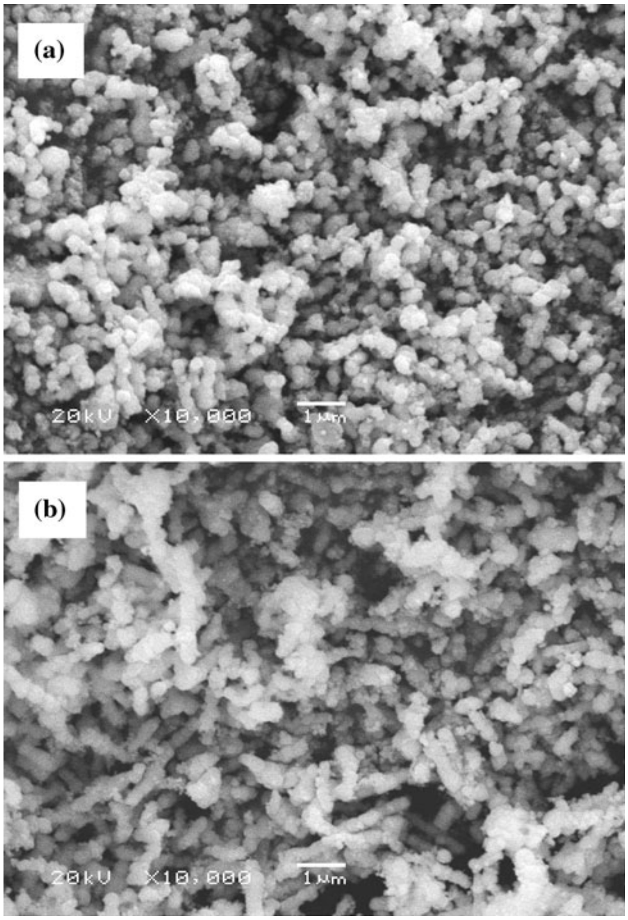

Fig. 4 SEM images of the electrode surface **a** with and **b** without magnetic field

50, and 100 mV s^{-1}. If the upper limit potential is lower than 0.2 V, the CVs show a roughly rectangular mirror image with respect to the zero-current line, which represents the electrical double-layer capacitive behavior of the NiO nanowire electrodes, as shown in the inset of Fig. 5a, b. If the upper potential is higher than 0.2 V, the CVs correspond to a redox capacitor. Through redox reactions, more capacitance can be stored in the bulk of the nickel oxide than in the electrical double layer. Clearly, the oxidation and reduction peaks are observed at 0.27 V (oxidation) and 0.13 V (reduction), respectively. Two strong current peaks were observed to indicate that the capacitance of the NiO nanowires mainly resulted from peseudocapacitive capacitance based on a fast redox mechanism. Two strong current peaks correspond to a redox reaction according to the following equation [27–29]:

$$\mathrm{NiO} + \delta\,\mathrm{OH}^- \leftrightarrow \delta\,\mathrm{NiOOH} + (1-\delta)\,\mathrm{NiO} + \delta\,e^- \quad (1)$$

Therefore, the capacitance of the NiO nanowire electrode is derived from a pseudocapacitive capacitance based on the obvious redox peaks. The oxidation and reduction peaks are symmetrical throughout the entire range of scan rates to indicate the good reversibility of the redox reactions at/near the electrode surface [30]. As the scan rate increased, the potential and the current at the two peaks shifted toward the positive and negative axes because of the abundant surface area [31] of the porous NiO nanowires and the fast ionic/electronic diffusion rate during the Faradaic redox reaction. The interface/surface structure and ionic/electronic diffusion, which significantly affect the rate capability and specific capacitance of the supercapacitor [32], are vital to the electrochemical electrode. Figure 5c presents the typical cyclic voltammograms of both MNiO and NiO electrodes in the potential region of −0.3 to 0.5 V at a scanning rate of 10 mV s^{-1}. In the 6 M KOH solution, the peak electric current on the electrode is larger than that on the bare electrode to indicate that the electrode produced in the added magnetic field has a significantly high electrochemical activity. The specific capacitance values were determined from the CV curves with the following equation:

$$C = \frac{1}{2 \cdot \Delta V \cdot m} \int_{V_{\mathrm{initial}}}^{V_{\mathrm{final}}} \frac{|I|}{\mathrm{d}V/\mathrm{d}t} \mathrm{d}V \quad (2)$$

where C is the specific capacitance, ΔV is the potential window, m is the mass of the electrode material, $V_{\mathrm{initial/final}}$ is the start/end potential in one cycle, $|I|$ is the instantaneous current at a given potential, and $\mathrm{d}V/\mathrm{d}t$ is the potential scan rate. The calculated specific capacitances are shown in Fig. 5d. The MNiO electrode shows a high specific capacity and rate capability. The MNiO electrode exhibits excellent capacitance because of two reasons. First, the directional alignment of the NiO nanowires along the added magnetic field facilitates good separation and less agglomeration at the electrode surface, and as a result, the effective specific surface area increases. Second, the ordered porous channels ensure retention and immersion of the electrolyte, serve as a favorable ion path for electrolyte penetration, and allow rapid ionic transport into the bulk of the NiO nanowires.

With the effect of the added magnetic field during electrode production considered, galvanostatic charge/discharge measurements were conducted in a 6 M KOH aqueous electrolyte. Galvanostatic charge/discharge curves under different charge/discharge current densities for the MNiO and NiO eclectrodes were obtained in a stable potential from −0.3 to 0.35 V, as shown in Fig. 6a, b.

The potential time profiles exhibited symmetric charge/discharge features because each curve had good charge–discharge voltage plateaus, which indicate that the capacitance of NiO was mainly obtained from pseudocapacitive capacitance based on a fast redox mechanism [33]. The galvanostatic discharge curves of the MNiO and NiO electrodes for various charge/discharge current densities are

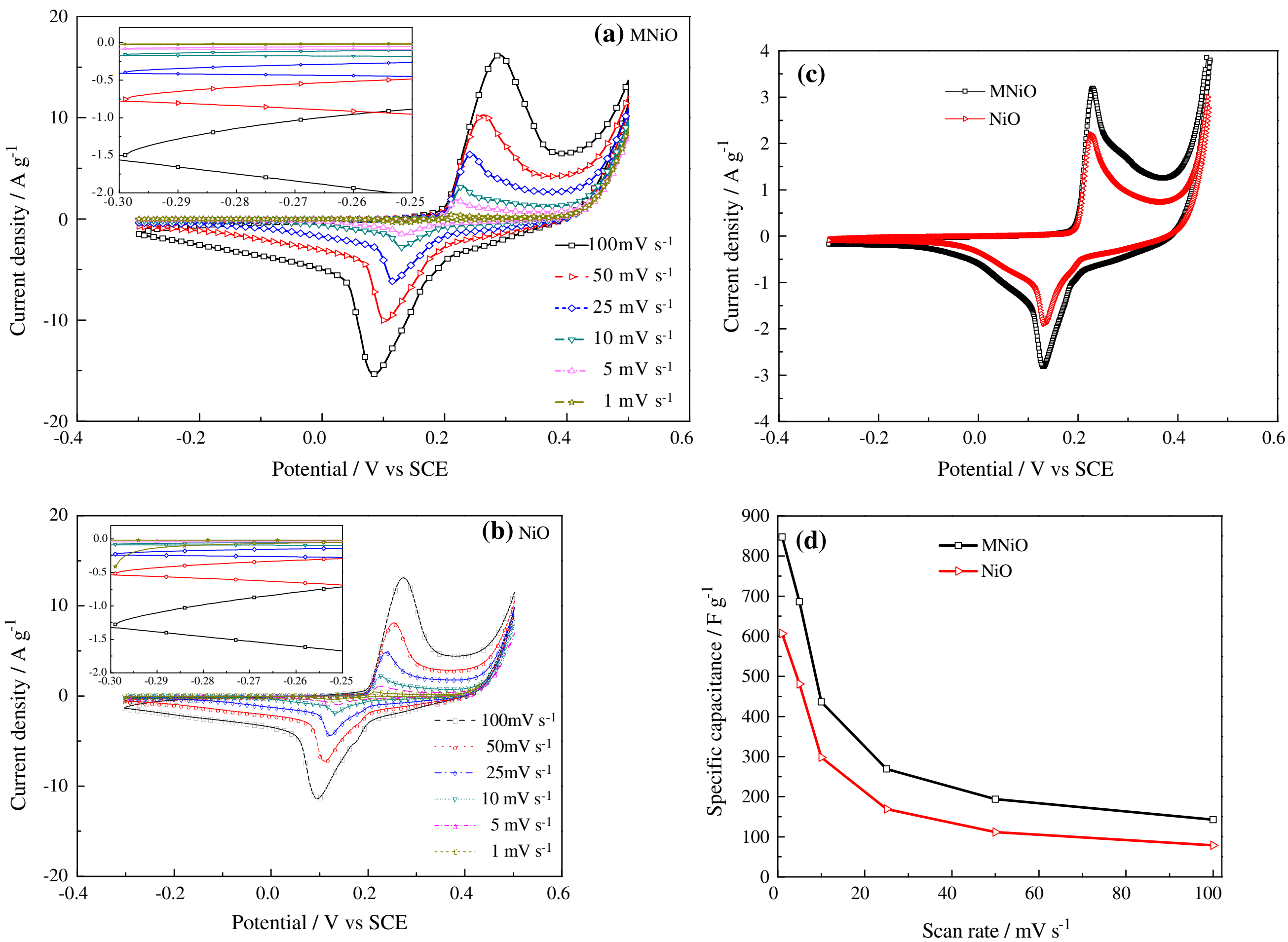

Fig. 5 Cyclic voltammetry curves and the specific capacitance of the electrode: **a** cyclic voltammetry curves of the MNiO electrode at different scan rates, **b** cyclic voltammetry curves of the NiO electrode at different scan rates, **c** cyclic voltammetry curves of the electrodes with and without the magnetic field at a scan rate of 10 mV/s, and **d** specific capacitance of the electrodes with and without a magnetic field at different scan rates derived from the cyclic voltammetry curves

shown in Fig. 6c, d. With the effect of the magnetic field considered, Fig. 6e presents the galvanostatic charge/discharge curves of the MNiO and NiO electrodes in the potential region of −0.3 to 0.35 V at a current density of 1 A g^{-1}. The result showed that compared with that of the NiO electrode, the discharge time increased after the magnetic field was added. The specific capacitance was derived from these discharges curves with the use of the following equation:

$$C = \frac{I \cdot \Delta t}{m \cdot \Delta V} \tag{3}$$

where C is the specific capacitance, I is the discharge current, ΔV is the potential window, Δt is the discharge time in the potential window, m is the mass of the active materials, and I/m is the discharge current density. The values are shown in Fig. 6f. The specific capacitance values of the MNiO and NiO electrode were 875 and 690 F g^{-1}, respectively, at a discharge current density of 0.1 A g^{-1}. The specific capacitance value of the electrode prepared with the magnetic field is higher than that prepared without the magnetic field. This result is consistent with the findings from the CV tests.

Energy and power densities are two important factors that affect the electrochemical performance of an electrode. The galvanostatic charge/discharge curves indicate that energy density and power density can be calculated via Eqs. (4) and (5) as follows:

$$D_e = \frac{1}{2} C (\Delta V)^2 \tag{4}$$

$$D_p = \frac{D_e}{\Delta t} \tag{5}$$

where D_e is the energy density, C is the specific capacitance, ΔV is the potential window of discharge, D_p is the power density, and Δt is the discharge time in the potential window. Figure 7a shows the maximum power density at 720 and 190 W kg^{-1}, with the highest energy densities of

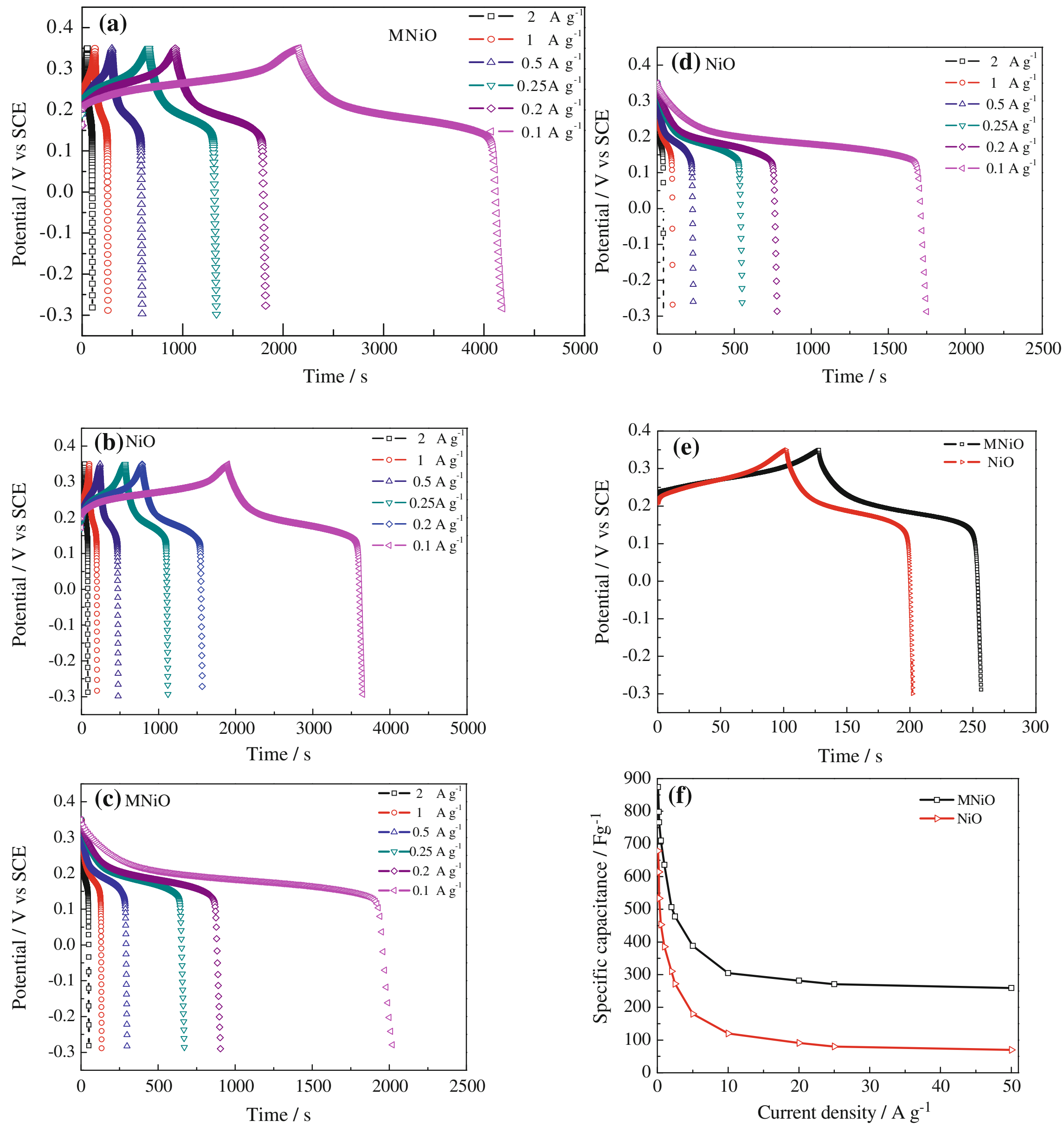

Fig. 6 Galvanostatic charge/discharge curves and specific capacitance for the electrode, **a** galvanostatic charge/discharge curves with different charge/discharge current densities for the MNiO electrode, **b** galvanostatic charge/discharge curves with different charge/discharge current densities for the NiO electrode, **c** galvanostatic discharge curves of the MNiO electrode for various charge/discharge current densities, **d** galvanostatic discharge curves of the NiO electrode for various charge/discharge current densities, **e** galvanostatic charge/discharge curves of the electrodes with and without the magnetic field at a charge/discharge current density of 10 mV/s, and **f** specific capacitance of the electrodes with and without the magnetic field at various charge/discharge current densities derived from the galvanostatic charge/discharge curves

27.2 and 6.1 Wh kg^{-1} obtained from the MNiO and NiO electrodes. The Ragone plot in Fig. 7b shows that the energy and power densities of the MNiO electrode were significantly higher than those of the NiO electrode. Although at a comparable power density, the energy density of the MNiO electrode was more than twice as high as that of the NiO electrode.

Since long life cycle is in the most important criterion for a supercapacitor, an endurance test of the electrodes was carried out by galvanostatic charge/discharge in the potential window from −0.3 to 0.35 V at 1 A g^{-1}. Figure 8 shows the relationship between capacitance retention and cycling number of both MNiO and NiO electrodes over 1,000 cycles. Two curves are almost the same; during the beginning cycle the specific capacitance increased, which resulted from the activation process of both the NiO electroactive materials on the electrode surface. It is obvious that the MNiO electrode exhibits better cycling

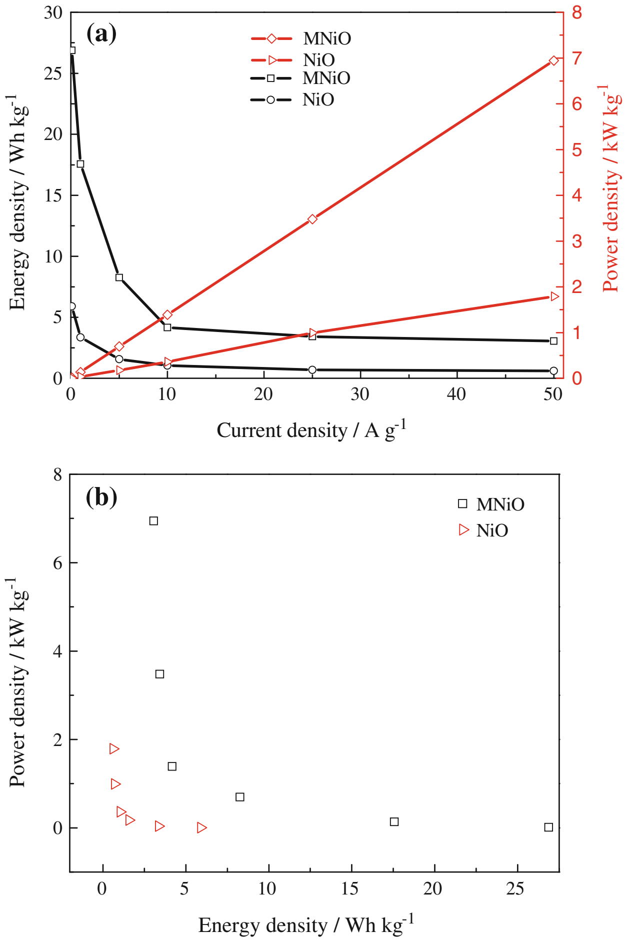

Fig. 7 Energy and power densities with various charge/discharge current densities and Ragone plots of the electrodes

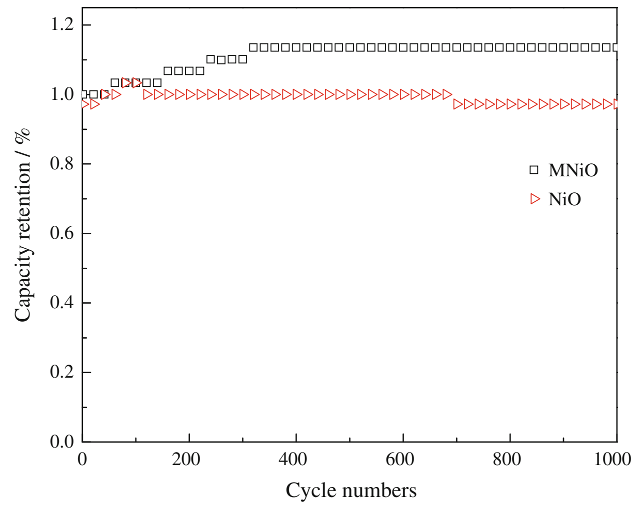

Fig. 8 Cycling performance of the MNiO and NiO electrodes

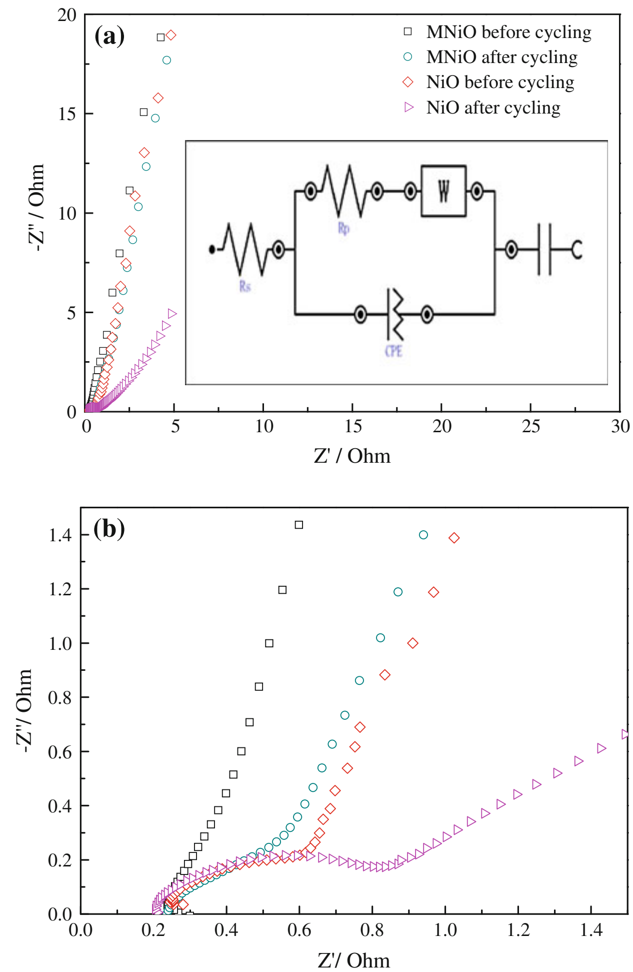

Fig. 9 Equivalent circuit of the MNiO and NiO electrodes

performance than NiO electrode, the MNiO electrode had no degradation after 1,000 continuous charge–discharge cycles at a current density of 1 A g^{-1}, owing to the orderly surface structure and orderly pole channel structure.

The detailed characteristics of the electrode can be observed by electrochemical impedance spectroscopy (EIS) analyzed via Nyquist plots with and without the magnetic field, which represent the imaginary part (Z'') and the real part (Z') of the impedance, respectively. Figure 9a shows the Nyquist plots of the EIS spectra of the electrode before and after 1,000 cycles at an applied potential of 0.25 V (vs. SCE). The semicircles in the high-frequency region and the slopes of the straight line in the low-frequency range were different. The inset of Fig. 9a shows the equivalent circuit derived from the Nyquist plots. R_s is the bulk solution resistance, R_{ct} is the Faradaic interfacial charge-transfer resistance, COE is the constant phase element that accounts for a double-layer capacitance, W is the Warburg impedance, and C_F is the Faradaic pseudocapacitor. Figure 9b shows the expanded plots at the high-frequency region. The bulk solution resistance R_s and the charge-transfer resistance R_{ct} can be obtained from the Nyquist plot, in which the high-frequency semicircle intercepts the real axis at R_s and ($R_s + R_{ct}$). Before cycling,

the bulk solution resistance had similar values of 0.14 Ω with and without the magnetic field; the corresponding charge-transfer resistances were 0.21 and 0.27 Ω, respectively, deduced from the enlarged figure shown in the inset of Fig. 9a. Faradaic interfacial charge-transfer resistance is a factor that limits the power density of pseudocapacitors [34]. The electrode with the magnetic field exhibits low charge-transfer resistance, which significantly improves the high power density of the pesudocapacitance [35]. After 1,000 cycles, R_{ct} increased and capacitance decreased, which may be due to the following reasons. First, the crack and loss of the active material [36, 37] on the electrode surface during the long cycling life test; as a result, the efficient mass of the NiO materials was reduced. Second, the structure and crystal form of the NiO nanomaterials had been changed when the Faraday reaction had taken place in the electrode during the charge–discharge cycles, which resulted in the decreased capacitance. Therefore, the R_{ct} increased, causing the electrochemical capacitance of the electrodes to decrease.

4 Conclusions

The addition of a magnetic field significantly affects the NiO electrode surface. The presence of the MNiO electrode in the magnetic field contributes to the ordered surface, large effective specific surface area, efficient transport channels, fast and high conductivity, and good chemistry stability of the electrodes of NiO capacitors. The MNiO electrode shows high specific capacitance (506 F g^{-1}), power density (135.8 W kg^{-1}), and energy density (17.6 Wh kg^{-1}). At 20 A g^{-1} current density, the capacitance of the MNiO electrode can be as high as 104.8 F g^{-1}. After a long cycle test in KOH solution, the electrode prepared in the magnetic field exhibits high and stable specific capacitance retention, which is an important requirement for supercapacitors. More importantly, an electrode with high electrochemical properties is developed, and a new method to utilize the magnetic field is introduced.

References

1. Bao LH, Zang JF, Li XD (2011) Nano Lett 11:1215–1220
2. Miller JR, Simon P (2008) Sci Mag 321:651–652
3. Conway BE (1997) Electrochemical supercapacitor: scientific fundamentals and technological applications. Kluwer Academic/Plenum Publishers, New York, p 3
4. Wu MS, Wang MJ, Jow JJ (2006) J Power Sour 195:1523–1532
5. Cao WJ, Zheng JP (2012) J Power Sour 213:180–185
6. Lee JW, Ahn T, Kim JH, Ko JM, Jim JD (2011) Electrochim Acta 56:4849–4875
7. Yuan CZ, Cao B, Shen LF, Yang SD, Hao L, LuX J, Zhang F, Zhang LJ, Zhang XG (2011) Nanoscale 3:29–545
8. Jiang H, Ma J, Li CZ (2012) Adv Mater 24:4197–4202
9. Hu CC, Chang KH, Lin MC, Wu YT (2006) Nano Lett 6:2690–2695
10. Matthew PY, Su D, Nebojsa SM, Teng XW (2012) J Electrochem Soc 159:A1598–A1603
11. Chen S, Zhu JW, Han QF, Zheng ZJ, Yang Y, Wang X (2009) J Cryst Growth 9:4356–4361
12. Hiraoka T, Izadi-Najafabadi A, Yamad AT, Futaba DN, Yasuda S, Tanaike O, Hatori H, Yumura M, Lijima S, Hata K (2010) Adv Mater 20:422–428
13. Cui ZM, Xing W, Liu CP, Tian D, Zhang H (2010) J Power Sour 195:1619–1623
14. Tarsame S, Sian Reddy GB (2004) Electrochim Acta 49:5223–5226
15. Mai YJ, Tu JP, Xia XH, Gu CD, Wang XL (2011) J Power Sour 196:6388–6393
16. Khomenko V, Raymundo PE, Beguin F (2006) J Power Sour 153:183–190
17. Kim YT, Tadai K, Mitani T (2005) J Mater Chem 46:4914–4921
18. Kong D, Wang JM, Shao HB, Zhang JQ, Cao CN (2011) J Pediatr Adolesc Gynecol 509:5611–5616
19. Arthur TS, Bates DJ, Cinigliano N, Johnson DC, Malati P, Mosby JM, Perre E, Rawls MT, Prieto AM, Dunn B (2011) MRS Bull 36:523–531
20. Toupin M, Brousse T, Belanger D (2004) Chem Mater 16:3184–3190
21. Xu CJ, Kang FY, Li BH, Du HD (2010) J Mater Res 25:1421–1432
22. Simon P, Gogotsi Y (2008) Nat Mater 7:845–854
23. Shao CL, Guan HY, Wen SB, Chen B, Han DX, Gong J, Yang XH, Liu YC (2004) Chem J Chin Univ 25:1013–1015
24. Liang K, Tang XZ, Hu WC (2012) J Mater Chem 22:11062–11607
25. Bund A, Koehler S, Kuehnlein HH, Plieth W (2003) Electrochim Acta 49:147–152
26. Jiang CX, Wang HY, Wang YZ, Chen XR, Tang YG (2013) J Power Sour 238:257–264
27. Yeagar MP, Su D, Marinkovic NS, Teng XW (2012) J Electrochem Soc 159:A1598–A1603
28. Chigane M, Ishikawa M (1994) J Electrochem Soc 141:3439–3443
29. Wang HB, Pan QM, Wang XP, Yin GP, Zhao JW (2009) J Appl Electrochem 39:1597–1602
30. Kim JH, Zhu K, Yan YF, Perkins CL (2010) Nano Lett 10:4099–4104
31. Olsen E, Thonstad J (1999) J Appl Electrochem 29:301–311
32. Wang DC, Ni WB, Pang H, Lu QY, Huang ZJ, Zhao JW (2010) Electrochim Acta 55:6830–6835
33. Gamby J, Taberna PL, Simon P, Fauvarque JF, Chesneau M (2010) J Power Sour 101:109–116
34. Bard AJ, Faulkner LR (2001) Electrochemical methods: fundamentals and applications. Wiley Press, New York, p 106
35. Zang JF, Bao SJ, Li CM, Bian HJ, Cui XQ, Bao QL, Sun CQ, Guo J, Lian K (2008) J Phys Chem C 112:14843–14847
36. Guo YG, Hu JS, Wan LJ (2008) Adv Mater 20:2965–2969
37. Wu MS, Huang YA, Yang CH (2008) J Electrochem Soc 155:A798–A805